Scaling and intermittency in compressible isotropic turbulence

Jianchun Wang*
Department of Physical Science and Engineering, Nagoya Institute of Technology, Nagoya 466-8555, Japan and Department of Mechanics and Aerospace Engineering, Southern University of Science and Technology, Shenzhen, Guangdong 518055, China

Toshiyuki Gotoh and Takeshi Watanabe
Department of Physical Science and Engineering, Nagoya Institute of Technology, Nagoya 466-8555, Japan
(Received 1 December 2016; published 26 May 2017)

Scaling and intermittency in compressible isotropic turbulence at the turbulent Mach number M_t ranging from 0.5 to 1.0 are studied by using numerical simulations with solenoidal forcing. Linear relations between the structure functions of the compressible velocity component and those of thermodynamic variables are modeled based on the shock jump conditions and are verified by numerical simulations. At a turbulent Mach number around 1.0, the relative scaling exponent of the structure functions saturates with an increase of the order. After proper normalization, the tails of the probability density functions (PDFs) of the increments of the compressible velocity component and thermodynamic variables overlap one another for different separations. Moreover, we study the conditional PDFs of the increments with respect to the shocklet. Linear relations between the tails of unconditional PDFs and conditional PDFs are established. The shocklet plays an important role in the determination of the PDF tails. The compressible velocity increment is decomposed into a negative component and a positive component. The negative component of the compressible velocity increment exhibits a scaling behavior with the saturation of the scaling exponent at high orders, which is similar to the Burgers turbulence, while the positive component of the compressible velocity increment exhibits a power-law scaling behavior, which is similar to the incompressible turbulence.

DOI: 10.1103/PhysRevFluids.2.053401

I. INTRODUCTION

The statistics of compressible turbulence has been the subject of extensive investigations [1–14] owing to its significant importance in many engineering applications and natural phenomena, including combustion, hypersonic flight, and astrophysics. The velocity dynamics is more complex in compressible turbulence than that in incompressible turbulence, due to the nonlinear interactions of vortices, shock waves, and expansionlike waves in compressible turbulence. In addition, there are strong couplings between the velocity field and thermodynamic fields in compressible turbulence. In this paper we study the scaling and intermittency of compressible turbulence when the turbulent Mach number increases from 0.5 to unity in the nonlinear subsonic regime.

The anomalous scaling behavior of structure functions is considered as a signature of the intermittency of turbulent statistics, which has attracted a great deal of attention in the research of incompressible turbulence. There also have been a number of studies on the intermittency of compressible turbulence, particularly in supersonic astrophysical flows. The occurrence of shock waves changes the Richardson-Kolmogorov picture of the energy cascade [15–18] and causes distinct intermittency in compressible turbulence [19–24]. Boldyrev *et al.* extended the phenomenological model of She and Leveque [25] to supersonic turbulence based on the assumption that the most

*wangjc@sustc.edu.cn

dissipative structures are sheets instead of filaments [19,20]. Their multifractal model was found to be in good agreement with numerical simulations of supersonic turbulence.

Kritsuk *et al.* [21] performed numerical simulations of supersonic isothermal Euler turbulence at root mean square Mach number around 6 and at grid resolutions up to 2048^2 points. They showed that the spectrum of velocity exhibits a $k^{-1.95}$ scaling in the inertial range. The Kolmogorov $k^{-5/3}$ scaling of the spectrum was recovered by the density-weighted velocity $\rho^{1/3}\mathbf{u}$, where ρ is the density and $\mathbf{u}$ is the velocity. Schmidt *et al.* [22] reported universal scaling exponents for the structure functions of density-weighted velocity $\rho^{1/3}\mathbf{u}$ in two different types of supersonic turbulence that were driven by solenoidal force and compressible force respectively at root mean square (rms) Mach number around 5.5. They also pointed out that the most intermittent dissipative structures of supersonic turbulence are shock waves, similar to the situation of Burgers turbulence.

Konstandin *et al.* studied the structure functions in both Lagrangian and Eulerian frameworks, by numerical simulations of supersonic turbulence at different gird resolutions: 256^3, 512^3, and 1024^3 [23]. They reported that both Lagrangian and Eulerian structure functions exhibit higher intermittency for compressible forcing as compared to the situation of solenoidal forcing. Federrath performed numerical simulations of isothermal supersonic Euler turbulence at grid resolutions of 256^3–4096^3 with Mach number 17, using two types of forces: solenoidal driving and compressible driving [24]. He confirmed the k^{-2} scaling of the pure velocity spectrum in the inertial range, which is close to Burgers turbulence. He also reported that there is a $k^{-1.74}$ scaling of the spectrum of the density-weighted velocity $\rho^{1/3}\mathbf{u}$ for solenoidal driving, close to incompressible turbulence. The density-weighted velocity $\rho^{1/3}\mathbf{u}$ was found to exhibit a $k^{-2.10}$ scaling in the inertial range for compressible driving.

In this paper we present a study of scaling and intermittency of velocity and thermodynamic variables in solenoidally forced compressible turbulence by numerical simulations at a grid resolution of 1024^3 and at different turbulent Mach numbers from $M_t = 0.5$ to $M_t = 1.0$. In Sec. II we provide a brief description of the physical governing equations and the numerical method. In Sec. III we present simulation parameters of the data base and some fundamental statistics of simulated flows. In Sec. IV we study the scaling behaviors of structure functions of the velocity and thermodynamic variables by the shock jump conditions [2,5] and the extended self-similarity analysis [26,27]. We also investigate the probability density functions (PDFs) of the increments of the compressible velocity component and thermodynamic variables by employing conditional statistics. In Sec. V we present a summary and the main conclusions of our study.

II. GOVERNING EQUATIONS AND NUMERICAL METHOD

Numerical simulations of compressible isotropic turbulence are performed in a cubic box of $2\pi^3$ with periodic boundary conditions. A hybrid compact weighted essentially nonoscillatory (WENO) scheme [28] is applied for the numerical simulations on a uniform grid with 1024^3 grid points. The hybrid scheme combines an eighth-order compact finite-difference scheme [29] for smooth regions and a seventh-order WENO scheme [30] for shock regions. Some grid refinement studies of the hybrid scheme for turbulent Mach number around 1.0 were performed in previous works [5,6].

A set of reference scales can be introduced to normalize the hydrodynamic and thermodynamic variables in compressible turbulence. The following reference variables are used: the reference length L_f, velocity U_f, density ρ_f, pressure $p_f = \rho_f U_f^2$, temperature T_f, energy per unit volume $\rho_f U_f^2$, viscosity μ_f, and thermal conductivity κ_f. After normalization, three reference governing parameters are obtained: the reference Reynolds number $\mathrm{Re} \equiv \rho_f U_f L_f/\mu_f$, the reference Mach number $M = U_f/c_f$, and the reference Prandtl number $\mathrm{Pr} \equiv \mu_f C_p/\kappa_f$. Here the speed of sound is defined by $c_f \equiv \sqrt{\gamma R T_f}$. In addition, $\gamma \equiv C_p/C_v$ is the ratio of specific heat at constant pressure C_p to that at constant volume C_v, which is assumed to be equal to 1.4. Further, R is the specific gas constant. The parameter α is defined by $\alpha \equiv \mathrm{Pr}\,\mathrm{Re}(\gamma - 1)M^2$. The parameter Pr is equal to 0.7.

The following dimensionless Navier-Stokes equations in conservation form are solved numerically:

$$\frac{\partial \rho}{\partial t} + \frac{\partial(\rho u_j)}{\partial x_j} = 0, \tag{1}$$

$$\frac{\partial(\rho u_i)}{\partial t} + \frac{\partial[\rho u_i u_j + p\delta_{ij}]}{\partial x_j} = \frac{1}{\mathrm{Re}}\frac{\partial \sigma_{ij}}{\partial x_j} + \mathcal{F}_i, \tag{2}$$

$$\frac{\partial \mathcal{E}}{\partial t} + \frac{\partial[(\mathcal{E}+p)u_j]}{\partial x_j} = \frac{1}{\alpha}\frac{\partial}{\partial x_j}\left(\kappa\frac{\partial T}{\partial x_j}\right) + \frac{1}{\mathrm{Re}}\frac{\partial(\sigma_{ij}u_i)}{\partial x_j} - \Lambda + \mathcal{F}_j u_j, \tag{3}$$

$$p = \rho T/\gamma M^2, \tag{4}$$

where ρ is the density, u_i is the velocity component, p is the pressure, and T is the temperature. Here $\mathcal{F}_i$ is a large-scale forcing to the fluid momentum and Λ is a large-scale cooling function per unit volume. The viscous stress σ_{ij} is defined by

$$\sigma_{ij} = \mu\left(\frac{\partial u_i}{\partial x_j} + \frac{\partial u_j}{\partial x_i}\right) - \frac{2}{3}\mu\theta\delta_{ij}, \tag{5}$$

where $\theta \equiv \partial u_k/\partial x_k$ is the normalized velocity divergence. The total energy per unit volume $\mathcal{E}$ is defined by

$$\mathcal{E} = \frac{p}{\gamma - 1} + \frac{1}{2}\rho(u_j u_j). \tag{6}$$

The Sutherland law is applied for the nondimensional temperature-dependent viscosity coefficient μ and thermal conductivity coefficient κ [28]. The velocity field is forced by fixing the energy spectrum within the two lowest wave-number shells. The force is only applied to the solenoidal component of velocity field. A uniform thermal cooling Λ is employed to sustain the internal energy in a statistically steady state [28].

III. ONE-POINT STATISTICS OF COMPRESSIBLE TURBULENCE

The Taylor microscale Reynolds number Re_λ and the turbulent Mach number M_t are defined, respectively, by [5]

$$\mathrm{Re}_\lambda = \mathrm{Re}\frac{\langle\rho\rangle u'\lambda}{\sqrt{3}\langle\mu\rangle}, \quad M_t = M\frac{u'}{\langle\sqrt{T}\rangle}, \tag{7}$$

where $\langle\,\rangle$ stands for an ensemble average. Here the rms velocity magnitude is $u' = \sqrt{\langle u_1^2 + u_2^2 + u_3^2\rangle}$ and the Taylor microscale is

$$\lambda = \sqrt{\frac{\langle u_1^2 + u_2^2 + u_3^2\rangle}{\langle(\partial u_1/\partial x_1)^2 + (\partial u_2/\partial x_2)^2 + (\partial u_3/\partial x_3)^2\rangle}}. \tag{8}$$

The Kolmogorov length scale η and the integral length scale L_I are defined, respectively, as

$$\eta = [\langle\mu/\mathrm{Re}\rho\rangle^3/\epsilon]^{1/4} \tag{9}$$

and

$$L_I = \frac{3\pi}{2(u')^2}\int_0^\infty \frac{E(k)}{k}dk, \tag{10}$$

where ϵ is the ensemble average of the dissipation rate per unit mass, $\epsilon = \langle\sigma_{ij}S_{ij}/\mathrm{Re}\rho\rangle$, and $E(k)$ is the spectrum of kinetic energy per unit mass, namely, $\int_0^\infty E(k)dk = (u')^2/2$. The strain rate tensor S_{ij} is defined by $S_{ij} = \frac{1}{2}(\frac{\partial u_i}{\partial x_j} + \frac{\partial u_j}{\partial x_i})$.

TABLE I. Simulation parameters and resulting flow statistics.

Resolution	Re_λ	M_t	$\eta/\Delta x$	L_I/η	λ/η	S_3	θ'	ω'	θ'/ω'
1024^3	253	0.51	1.00	233	31.2	−0.53	1.7	26.9	0.065
1024^3	262	0.60	1.02	231	31.6	−0.53	2.8	25.3	0.11
1024^3	261	0.79	1.05	229	30.9	−0.83	4.8	23.7	0.20
1024^3	250	1.02	1.04	226	29.1	−1.95	8.2	23.7	0.35

The overall statistics for simulated compressible flows are summarized in Table I. The grid resolution is 1024^3 and the Taylor microscale Reynolds number is about 250. Four different turbulent Mach numbers are considered: $M_t = 0.5$, 0.6, 0.8, and 1.0, corresponding to the different levels of compressibility. The resolution parameter $\eta/\Delta x$ is in the range $1.0 \leqslant \eta/\Delta x \leqslant 1.05$ in our simulations, where Δx denotes the grid length in each direction. Consequently, the resolution parameter $k_{\max}\eta$ is in the range $3.1 \leqslant k_{\max}\eta \leqslant 3.3$, where the largest wave number $k_{\max}$ is half of the number of grids N in each direction: $k_{\max} = N/2 = \pi/\Delta x$. In previous works, grid refinement convergence studies were carried out at turbulent Mach number $M_t = 1.0$ [5,6]. The resolutions of $k_{\max}\eta \geqslant 3.1$ are enough for the convergence of small-scale statistics, including the kinetic energy spectrum at different wave numbers and the PDFs of velocity divergence and vorticity.

The velocity derivative skewness S_3 is defined as

$$S_3 = \frac{[\langle(\partial u_1/\partial x_1)^3 + (\partial u_2/\partial x_2)^3 + (\partial u_3/\partial x_3)^3\rangle]/3}{\{\langle(\partial u_1/\partial x_1)^2 + (\partial u_2/\partial x_2)^2 + (\partial u_3/\partial x_3)^2\rangle/3\}^{3/2}}. \tag{11}$$

For $M_t = 0.5$ and 0.6, the values of S_3 are similar to the typical values of -0.6 to -0.4 in incompressible turbulence [31]. The magnitude of S_3 becomes larger as M_t increases, for $M_t = 0.8$ and $M_t = 1.0$, due to the effect of shocklets [5,6]. Root mean square values of velocity divergence and vorticity magnitude are calculated as $\theta' = \sqrt{\langle\theta^2\rangle}$ and $\omega' = \sqrt{\langle\omega_1^2 + \omega_2^2 + \omega_3^2\rangle}$, respectively. The effect of turbulent Mach number on ω' is very small. Here θ' increases with the increase of M_t, which is consistent with a previous study of compressible turbulence [9].

We plot contours of the normalized velocity divergence θ/θ' on an arbitrarily selected x-y slice, at turbulent Mach numbers $M_t = 0.5$, 0.6, 0.8, and 1.0, in Fig. 1. At $M_t = 0.5$, high-expansion regions $\theta/\theta' \geqslant 2.0$ tend to be bloblike round structures. High-compression regions $\theta/\theta' \leqslant -2.0$ are narrower and longer than high-expansion regions at $M_t = 0.5$. As the turbulent Mach number M_t increases from $M_t = 0.5$, the high-compression regions become much narrower, indicating that high-compression motion of the flow is concentrated in smaller regions at higher turbulent Mach number. At $M_t = 1.0$, there are bandlike structures of high-compression regions, which represent shocklets [5,28]. We also observe that high-expansion regions $\theta/\theta' \geqslant 2.0$ become very rare at $M_t = 1.0$, indicating that expansion motion is weaker than compression motion in compressible turbulence at moderate and high turbulent Mach numbers [6,9].

We show isosurfaces of the velocity divergence, the density gradient, the pressure gradient, and the temperature gradient, respectively, at the levels $\theta = -8\theta'$, $|\nabla\rho| = 6|\nabla\rho|^{\mathrm{rms}}$, $|\nabla p| = 6|\nabla p|^{\mathrm{rms}}$, and $|\nabla T| = 6|\nabla T|^{\mathrm{rms}}$ in Fig. 2. Here the superscript rms represents the root mean square value, namely, $|\nabla\rho|^{\mathrm{rms}} = \langle\nabla\rho\cdot\nabla\rho\rangle^{1/2}$, $|\nabla p|^{\mathrm{rms}} = \langle\nabla p\cdot\nabla p\rangle^{1/2}$, and $|\nabla T|^{\mathrm{rms}} = \langle\nabla T\cdot\nabla T\rangle^{1/2}$. We observe sheetlike structures of the velocity divergence, which represent the shocklet structures at a very-high-compression level $\theta = -8\theta'$ [5,6]. The isosurfaces of the density gradient, the pressure gradient, and the temperature gradient are also sheetlike, which are similar to isosurfaces of velocity divergence. The small differences in the spatial distribution of the four physical variables are highlighted by a circle in each panel. Since there are jumps of pressure, density, and temperature across shocklets, it is reasonable that the singular structures of high compression, high-pressure

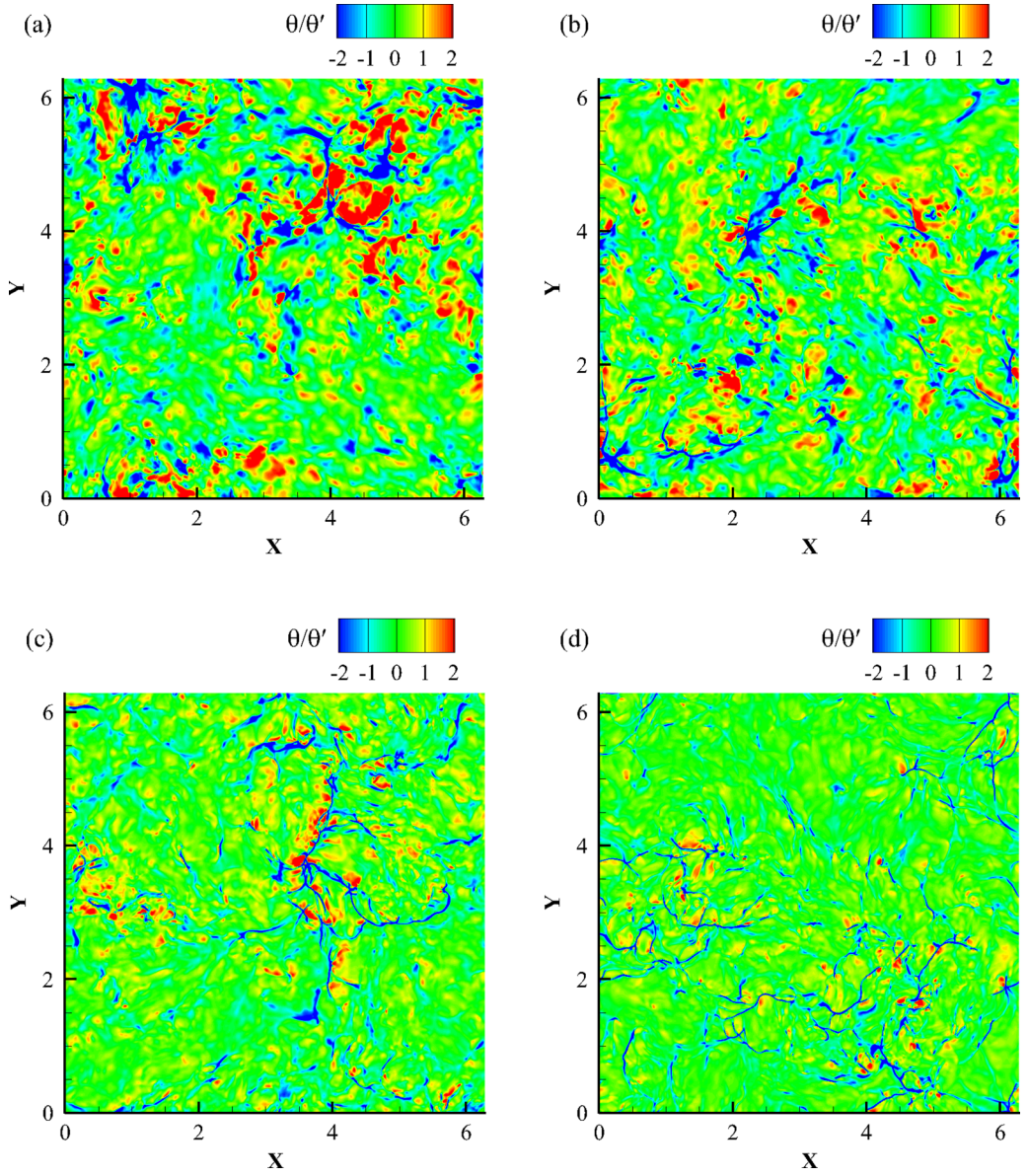

FIG. 1. Contours of the normalized velocity divergence θ/θ' on an arbitrarily selected x-y slice, at turbulent Mach numbers (a) $M_t = 0.5$, (b) $M_t = 0.6$, (c) $M_t = 0.8$, and (d) $M_t = 1.0$.

gradient, high-density gradient, and high-temperature gradient are almost identical and are nearly two dimensional.

IV. STRUCTURE FUNCTIONS OF VELOCITY AND THERMODYNAMIC VARIABLES

We employ the Helmholtz decomposition to decompose the velocity field into a solenoidal component $\mathbf{u}^s$ and a compressible component $\mathbf{u}^c$: $\mathbf{u} = \mathbf{u}^s + \mathbf{u}^c$, where $\nabla \cdot \mathbf{u}^s = 0$ and

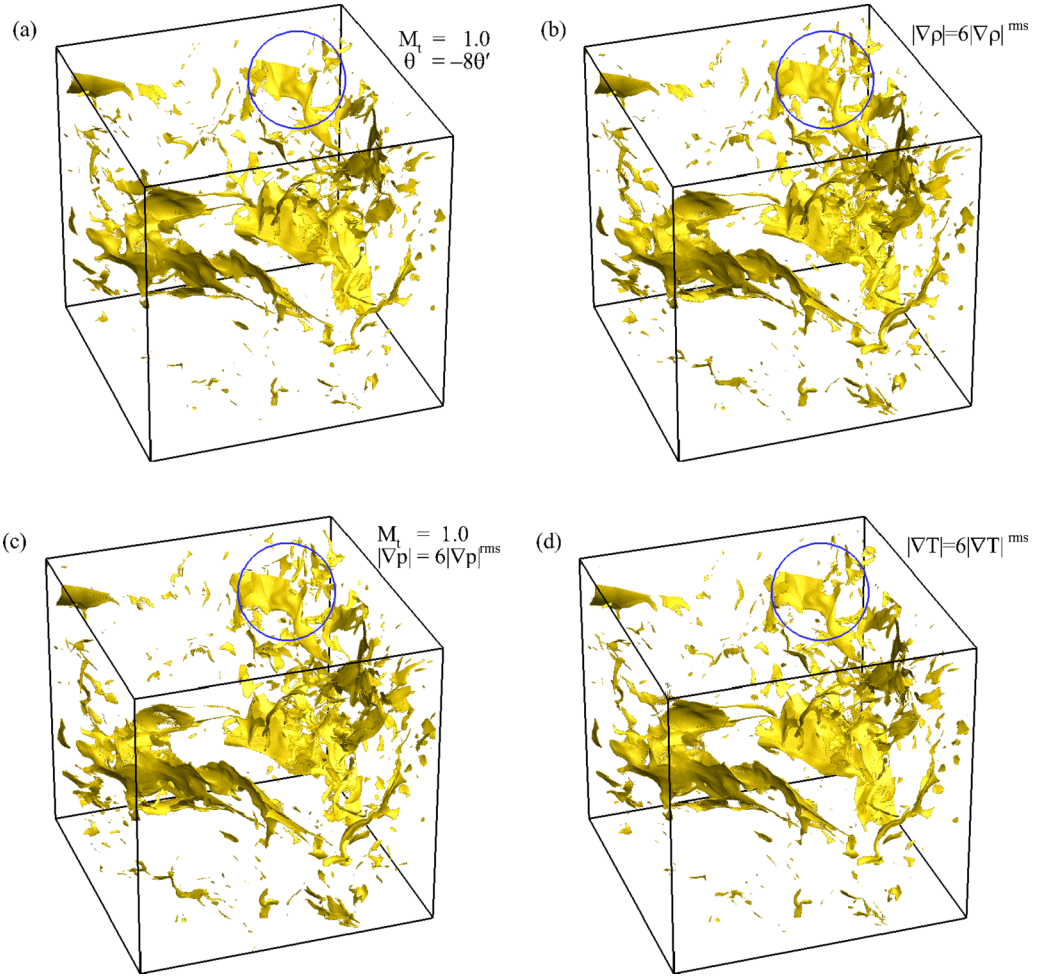

FIG. 2. Isosurfaces in a 512^3 subdomain of the 1024^3 simulation, at turbulent Mach number 1.0: (a) the velocity divergence, (b) the magnitude of the density gradient, (c) the magnitude of the pressure gradient, and (d) the magnitude of the temperature gradient. A circle is plotted in each panel to highlight the small differences in the spatial distribution of the four physical variables.

$\nabla \times \mathbf{u}^c = 0$ [1,2,6,9]. We define longitudinal structure functions for the velocity and its two components by

$$S_n^L(r) \equiv \left\langle \left| \frac{\delta_r u}{u'} \right|^n \right\rangle, \tag{12}$$

$$S_n^{L,s}(r) \equiv \left\langle \left| \frac{\delta_r u^s}{u'} \right|^n \right\rangle, \tag{13}$$

$$S_n^{L,c}(r) \equiv \left\langle \left| \frac{\delta_r u^c}{u'} \right|^n \right\rangle, \tag{14}$$

where $\delta_r u = [\mathbf{u}(\mathbf{x}+\mathbf{r}) - \mathbf{u}(\mathbf{x})] \cdot \hat{\mathbf{r}}$, $\delta_r u^s = [\mathbf{u}^s(\mathbf{x}+\mathbf{r}) - \mathbf{u}^s(\mathbf{x})] \cdot \hat{\mathbf{r}}$, and $\delta_r u^c = [\mathbf{u}^c(\mathbf{x}+\mathbf{r}) - \mathbf{u}^c(\mathbf{x})] \cdot \hat{\mathbf{r}}$ are the longitudinal increments of the velocity and its two components for the separation $\mathbf{r}$. Here $\hat{\mathbf{r}} = \mathbf{r}/|\mathbf{r}|$. We have performed normalization by using the rms velocity u'.

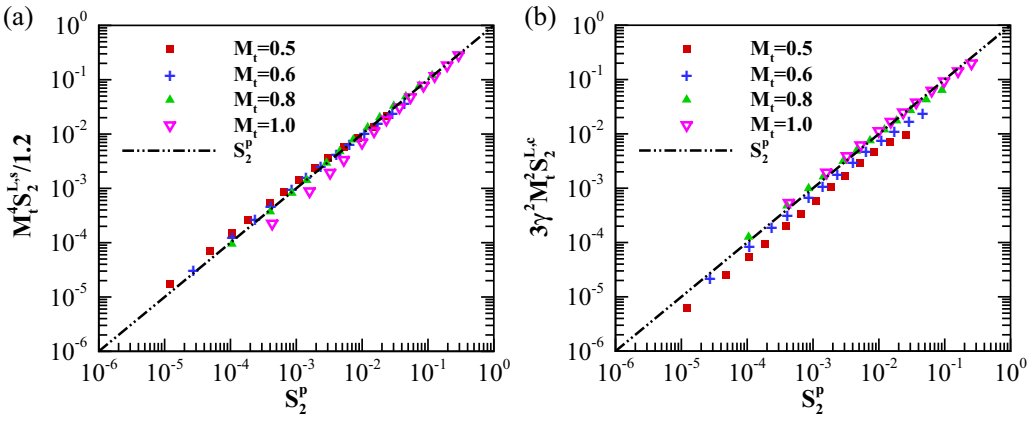

FIG. 3. (a) Normalized second-order structure function of the solenoidal velocity component versus the second-order structure function of the pressure. (b) Normalized second-order structure function of the compressible velocity component versus the second-order structure function of the pressure.

Similarly, we define structure functions for the density, pressure, and temperature as

$$S_n^{\rho}(r) \equiv \left\langle \left| \frac{\delta_r \rho}{\rho_0} \right|^n \right\rangle, \tag{15}$$

$$S_n^{p}(r) \equiv \left\langle \left| \frac{\delta_r p}{p_0} \right|^n \right\rangle, \tag{16}$$

$$S_n^{T}(r) \equiv \left\langle \left| \frac{\delta_r T}{T_0} \right|^n \right\rangle, \tag{17}$$

where $\delta_r \rho = \rho(\mathbf{x}+\mathbf{r}) - \rho(\mathbf{x})$, $\delta_r p = p(\mathbf{x}+\mathbf{r}) - p(\mathbf{x})$, and $\delta_r T = T(\mathbf{x}+\mathbf{r}) - T(\mathbf{x})$ are, respectively, the increments of the density, pressure, and temperature for the separation $\mathbf{r}$. The ensemble-average values of the thermodynamic variables ρ_0, p_0, and T_0 are used to normalize the structure functions.

If there are power-law scaling behaviors of the structure functions, we denote the power scaling exponents by ζ_n^L, $\zeta_n^{L,s}$, $\zeta_n^{L,c}$, ζ_n^{ρ}, ζ_n^{p}, and ζ_n^{T}, for the velocity, two components of velocity, density, pressure, and temperature, respectively: $S_n^L(r) \sim r^{\zeta_n^L}$, $S_n^{L,s}(r) \sim r^{\zeta_n^{L,s}}$, $S_n^{L,c}(r) \sim r^{\zeta_n^{L,c}}$, $S_n^{\rho}(r) \sim r^{\zeta_n^{\rho}}$, $S_n^{p}(r) \sim r^{\zeta_n^{p}}$, and $S_n^{T}(r) \sim r^{\zeta_n^{T}}$.

In Fig. 3(a) we plot the normalized second-order structure function of the solenoidal velocity component against the second-order structure function of the pressure. The relative scaling behavior is quite clear: $M_t^4 S_2^{L,s} \approx C_0^{(u^s,p)} S_2^p$, where $C_0^{(u^s,p)} = 1.2$. We note that $M_t^2 p_0/u'^2 = \rho_0/\gamma$ and $\rho_0 = 1$. Thus, the linear relation between $S_2^{L,s}$ and S_2^p supports the relation $\delta_r u^s \sim \delta_r p$, which is similar to the situation of incompressible turbulence [32].

We depict the normalized second-order structure function of the compressible velocity component versus the second-order structure function of the pressure in Fig. 3(b). Provided that the jumps across shocklets have major contributions to the fluctuations of the compressible velocity, we can model the compressible velocity increment based on the shock relation. The shocklets are defined based on two criteria, $\nabla^2 \rho = 0$ and $\theta < -R_\theta \theta'$, namely, the surface elements where the density exhibits inflection along the local normal and the compression rate is strong, where the threshold $R_\theta = 3$ [2,5]. We denote the variables upstream of a shocklet (lower-density side) by subscript 1 and downstream of a shocklet (higher-density side) with subscript 2. Thus, the density ratio $\rho_r = \rho_2/\rho_1 > 1$ and the pressure ratio $p_r = p_2/p_1 > 1$ across a shocklet.

According to ideal shock relationship, the jump of normal velocity across a shocklet can be written as [5,14]

$$\delta_s u_n = \sqrt{\frac{2(p_2 - p_1)^2}{\rho_1[(\gamma+1)p_2 + (\gamma-1)p_1]}}, \tag{18}$$

where $\delta_s u_n = |u_{2n} - u_{1n}|$. Here u_{1n} (u_{2n}) is the velocity, projected along the shock normal direction, upstream (downstream) of a shocklet relative to the shocklet front. The normal direction of a shocklet is along the density gradient vector and points to the side of smaller density [5].

For the situation of the weak shocklet, we assume that $\rho_1 \approx \rho_2 \approx \rho_0$, $p_1 \approx p_2 \approx p_0$, and $T_1 \approx T_2 \approx T_0$. Approximately, we obtain

$$\delta_s u_n \approx \frac{u'}{\gamma M_t}\frac{\delta_s p}{p_0}, \tag{19}$$

where $\delta_s p = p_2 - p_1$. The linear approximation (19) was verified for weak shocklets in a previous study of compressible isotropic turbulence at M_t from 0.5 to 1.0 [14]. It was shown that three PDFs of the jumps of the velocity, normal velocity component, and normal compressible velocity component across a shocklet almost collapse onto one another at $M_t = 0.8$ and 1.0 [14]. It is reasonable to assume that the jump of the compressible velocity component is equal to the jump of the velocity across a shocklet. Thus, we obtain $\gamma M_t \delta_s u^c/u' \approx \delta_s p/p_0$. We also assume the isotropy of the compressible velocity increment, namely, $|\mathbf{u}^c(\mathbf{x}+\mathbf{r}) - \mathbf{u}^c(\mathbf{x})| \sim \sqrt{3}[\mathbf{u}^c(\mathbf{x}+\mathbf{r}) - \mathbf{u}^c(\mathbf{x})] \cdot \hat{\mathbf{r}}$. Thus, we present the following approximations:

$$\frac{\sqrt{3}\gamma M_t \delta_r u^c}{u'} \approx \frac{\delta_r p}{p_0}. \tag{20}$$

We show that at high turbulent Mach numbers $M_t = 0.8$ and 1.0, the second-order structure functions of the compressible velocity component and pressure obey the linear relation quite well:

$$(\sqrt{3}\gamma M_t)^2 S_2^{L,c} \approx S_2^p. \tag{21}$$

For low turbulent Mach numbers $M_t = 0.5$ and 0.6, $(\sqrt{3}\gamma M_t)^2 S_2^{L,c}$ is still proportional to, but slightly smaller than, S_2^p. The deviations of numerical results from the approximation (21) can be explained by the following reason: At $M_t = 0.5$ and 0.6, the assumption $\delta_s u^c \approx \delta_s u$ is no longer accurate, which can be attributed to the weak strength of shocklet, viscosity effect, and fluctuations of the solenoidal velocity component [14].

The Rankine-Hugoniot jump condition for the relation between the density ratio and the pressure ratio across a shocklet can be written as [2,5]

$$\rho_r = \frac{(\gamma+1)p_r + \gamma - 1}{(\gamma-1)p_r + \gamma + 1}. \tag{22}$$

For a weak shocklet, we have the following linear approximation:

$$\frac{\delta_s \rho}{\rho_0} \approx \frac{1}{\gamma}\frac{\delta_s p}{p_0}, \tag{23}$$

where $\delta_s \rho = \rho_2 - \rho_1$. Based on the state equation of thermodynamic variables, the linear approximation of $\delta_s T = T_2 - T_1$ can be written as

$$\frac{\delta_s T}{T_0} \approx \frac{\gamma - 1}{\gamma}\frac{\delta_s p}{p_0}. \tag{24}$$

Linear approximations (23) and (24) were verified for weak shocklets in a previous study of compressible isotropic turbulence at M_t from 0.5 to 1.0 [14].

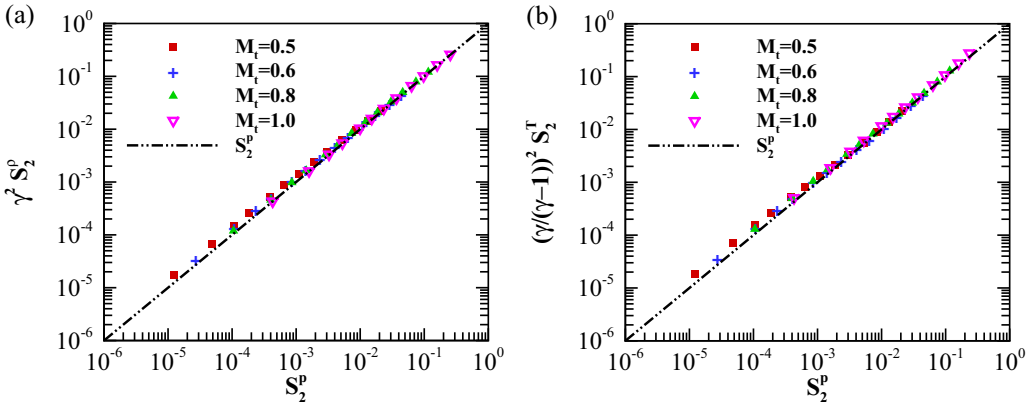

FIG. 4. (a) Normalized second-order structure function of the density versus the second-order structure function of the pressure. (b) Normalized second-order structure function of the temperature versus the second-order structure function of the pressure.

We propose the following relations for the increments of the density, temperature, and pressure:

$$\frac{\gamma \delta_r \rho}{\rho_0} \sim \frac{\delta_r p}{p_0} \tag{25}$$

and

$$\frac{\gamma \delta_r T}{(\gamma-1)T_0} \sim \frac{\delta_r p}{p_0}. \tag{26}$$

We plot the normalized second-order structure functions of the density and temperature versus the second-order structure function of the pressure in Fig. 4. It is found that the linear relations hold in the entire range of the separation:

$$\gamma^2 S_2^\rho \approx S_2^p \tag{27}$$

and

$$[\gamma/(\gamma-1)]^2 S_2^T \approx S_2^p. \tag{28}$$

To clarify the effect of shocklets on the statistical characteristics of the velocity and thermodynamic variables, we consider the conditional structure functions of the velocity and its two components:

$$J_n^L(r) \equiv \left\langle \left| \frac{1}{u'}[\mathbf{u}(\mathbf{x}+\mathbf{r}/2) - \mathbf{u}(\mathbf{x}-\mathbf{r}/2)] \cdot \hat{\mathbf{r}} \right|^n \middle| \nabla^2\rho(\mathbf{x}) = 0, \theta(\mathbf{x}) < -R_\theta \theta' \right\rangle, \tag{29}$$

$$J_n^{L,s}(r) \equiv \left\langle \left| \frac{1}{u'}[\mathbf{u}^s(\mathbf{x}+\mathbf{r}/2) - \mathbf{u}^s(\mathbf{x}-\mathbf{r}/2)] \cdot \hat{\mathbf{r}} \right|^n \middle| \nabla^2\rho(\mathbf{x}) = 0, \theta(\mathbf{x}) < -R_\theta \theta' \right\rangle, \tag{30}$$

$$J_n^{L,c}(r) \equiv \left\langle \left| \frac{1}{u'}[\mathbf{u}^c(\mathbf{x}+\mathbf{r}/2) - \mathbf{u}^c(\mathbf{x}-\mathbf{r}/2)] \cdot \hat{\mathbf{r}} \right|^n \middle| \nabla^2\rho(\mathbf{x}) = 0, \theta(\mathbf{x}) < -R_\theta \theta' \right\rangle, \tag{31}$$

where the conditions $\nabla^2\rho(\mathbf{x}) = 0$ and $\theta(\mathbf{x}) < -R_\theta\theta'$ were used to detect the shocklet from the compressible turbulent flows [2,5,14]. Here R_θ is set to 3 unless noted otherwise. Similarly, the conditional structure functions of the density, pressure, and temperature are

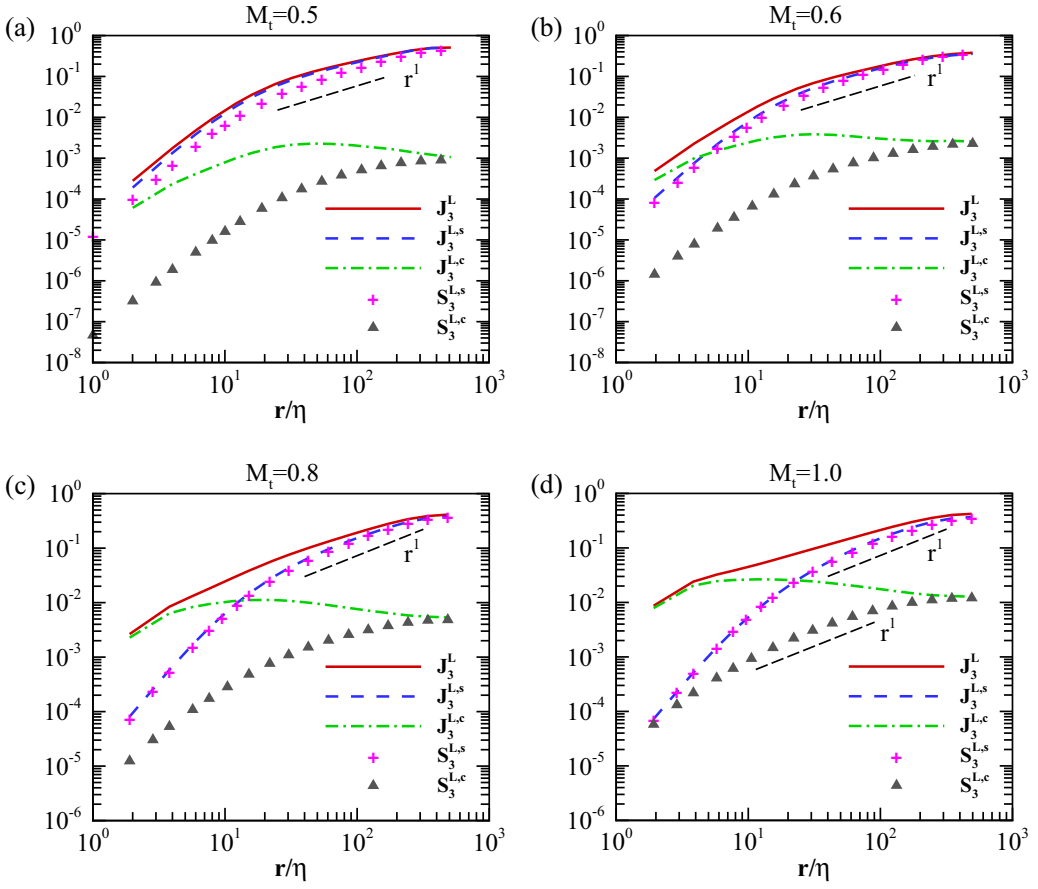

FIG. 5. Third-order conditional and unconditional structure functions of the velocity and its two components at (a) $M_t = 0.5$, (b) $M_t = 0.6$, (c) $M_t = 0.8$, and (d) $M_t = 1.0$.

defined as

$$J_n^{\rho}(r) \equiv \left\langle \left| \frac{1}{\rho_0}[\rho(\mathbf{x}+\mathbf{r}/2) - \rho(\mathbf{x}-\mathbf{r}/2)] \right|^n \middle| \nabla^2\rho(\mathbf{x}) = 0, \theta(\mathbf{x}) < -R_\theta\theta' \right\rangle, \tag{32}$$

$$J_n^{p}(r) \equiv \left\langle \left| \frac{1}{p_0}[p(\mathbf{x}+\mathbf{r}/2) - p(\mathbf{x}-\mathbf{r}/2)] \right|^n \middle| \nabla^2\rho(\mathbf{x}) = 0, \theta(\mathbf{x}) < -R_\theta\theta' \right\rangle, \tag{33}$$

$$J_n^{T}(r) \equiv \left\langle \left| \frac{1}{T_0}[T(\mathbf{x}+\mathbf{r}/2) - T(\mathbf{x}-\mathbf{r}/2)] \right|^n \middle| \nabla^2\rho(\mathbf{x}) = 0, \theta(\mathbf{x}) < -R_\theta\theta' \right\rangle. \tag{34}$$

If the fluctuation of a variable Q in smooth region is very small compared to the jump $\delta_s Q$ across shocklets, then we should observe a constant behavior of the conditional structure functions: $J_n^Q(r) \sim$ const. Moreover, the fluctuation of the variable Q is characterized by $Q(\mathbf{x}+\mathbf{r}) - Q(\mathbf{x}) \sim$ const when there is a shocklet located between $\mathbf{x}+\mathbf{r}$ and $\mathbf{x}$.

We present the third-order conditional structure functions and unconditional structure functions of the velocity and its two components, J_3^L, $J_3^{L,s}$, $J_3^{L,c}$, $S_3^{L,s}$, and $S_3^{L,c}$ in Fig. 5. We do not plot S_3^L in the figure since S_3^L is similar to $S_3^{L,s}$. The third-order conditional structure function $J_3^{L,s}$ of the solenoidal velocity component is found to be independent of the turbulent Mach number and is almost the same as $S_3^{L,s}$, indicating that the effect of the shocklet on the solenoidal velocity field is negligibly

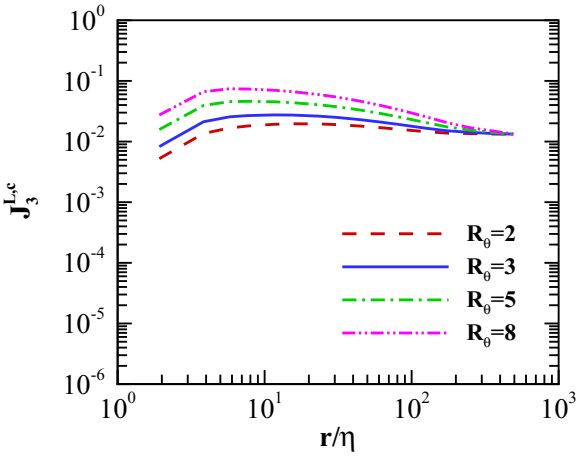

FIG. 6. Third-order conditional structure functions of the compressible velocity at $M_t = 1.0$ for different threshold R_θ.

small. This observation is consistent with previous studies of compressible turbulence at $M_t = 1.0$ [5]. In contrast, the third-order conditional structure function $J_3^{L,c}$ of the compressible velocity component highly depends on the turbulent Mach number: $J_3^{L,c}$ increases rapidly as M_t becomes larger. We observe that the third-order conditional structure function J_3^L of the velocity increases with turbulent Mach number at small scales. At $M_t = 1.0$, the compressible component dominates over the solenoidal component at small scales, $J_3^{L,c} > J_3^{L,s}$ at $r/\eta \leqslant 10$, while the solenoidal component dominates over the compressible component at large scales, $J_3^{L,c} < J_3^{L,s}$ at $r/\eta \geqslant 50$.

We find that the third-order unconditional structure function of the compressible velocity $S_3^{L,c}$ is always much smaller than its solenoidal counterpart $S_3^{L,s}$, except at dissipation scales $r/\eta \leqslant 2.0$ for $M_t = 1.0$. We also observe that at large scales $r/\eta \geqslant 300$, $S_3^{L,c}$ is almost equal to $J_3^{L,c}$, indicating the negligible effect of the shocklet at large scales. As the separation r decreases, the difference between $S_3^{L,c}$ and $J_3^{L,c}$ becomes larger, as a manifestation of the larger impact of shocklet at smaller scales. The difference between $S_3^{L,c}$ and $J_3^{L,c}$ also increases with the increase of turbulent Mach number. In particular, the curve $S_3^{L,c}$ becomes more flat as the turbulent Mach number increases. At $M_t = 1.0$, the curve $J_3^{L,c}$ only has a slight dependence on the separation r. We do not observe a clear power-law scaling region for $S_3^{L,c}$ at $M_t = 1.0$. We also plot a line of the r^1 scaling in the same figure.

We will now address the effect of threshold R_θ on the third-order conditional structure function of the compressible velocity $J_3^{L,c}$. We plot $J_3^{L,c}$ at $M_t = 1.0$ for four thresholds $R_\theta = 2$, 3, 5, and 8 in Fig. 6. We observe that $J_3^{L,c}$ becomes larger as R_θ increases for $r/\eta \leqslant 300$. The observation is reasonable since higher compression associated with the stronger shocklet gives rise to larger increments of the compressible velocity across the shocklet. The effect of threshold R_θ is more significant at smaller scales and is negligible at large scales $r/\eta \geqslant 300$.

We plot the normalized third-order conditional and unconditional structure functions of the pressure, density, and temperature J_3^p, $\gamma^3 J_3^\rho$, $[\gamma/(\gamma-1)]^3 J_3^T$, S_3^p, $\gamma^3 S_3^\rho$, and $[\gamma/(\gamma-1)]^3 S_3^T$, respectively, in Fig. 7. The coefficients γ^3 and $[\gamma/(\gamma-1)]^3$ are determined based on the relations (25) and (26). The relations (25) and (26) are confirmed again by the overlap of the three curves of the normalized structure functions of the pressure, density, and temperature. All of the third-order functions of the thermodynamic variables increase with the increase of turbulent Mach number. Similar to the situation of the compressible velocity, the difference between conditional and

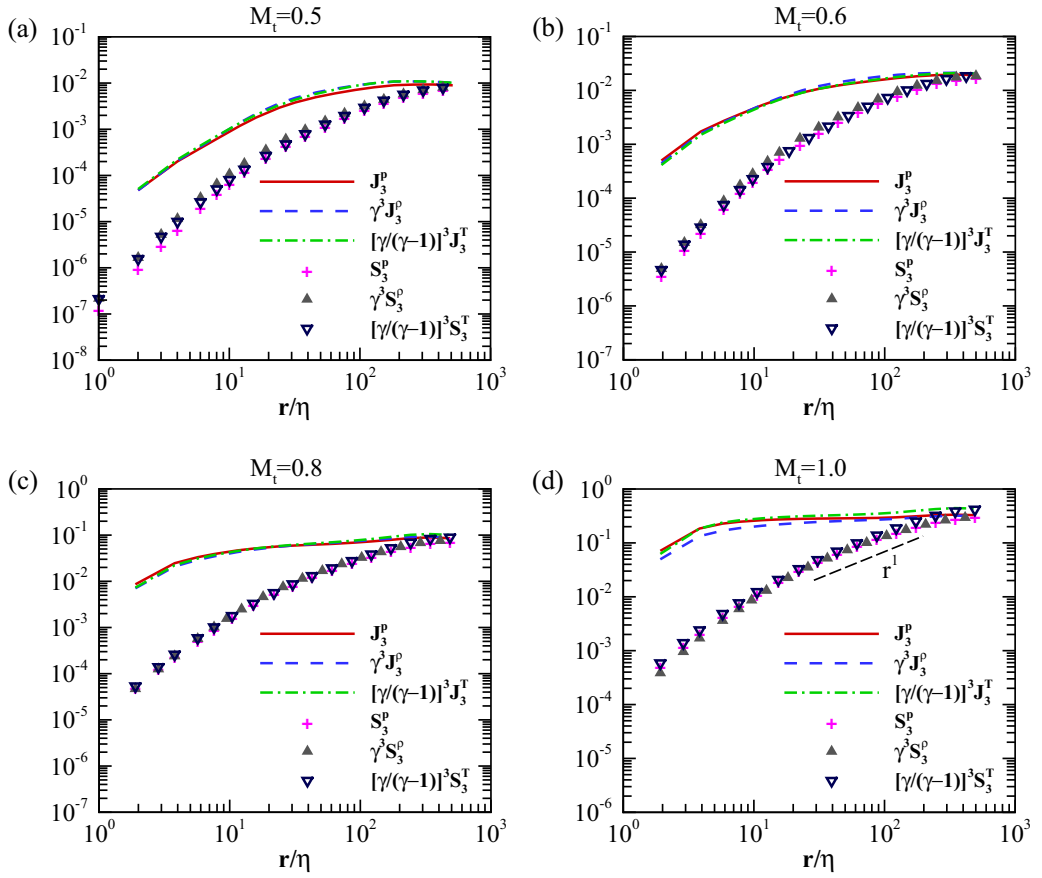

FIG. 7. Normalized third-order conditional and unconditional structure functions of the thermodynamic variables at (a) $M_t = 0.5$, (b) $M_t = 0.6$, (c) $M_t = 0.8$, and (d) $M_t = 1.0$.

unconditional structure functions is negligible at large scales $r/\eta \geqslant 300$ and becomes larger with the decrease of separation r and with the increase of turbulent Mach number M_t. We observe that plateau regions of the conditional structure functions develop gradually as M_t increases from 0.5 to 1.0. In particular, at $M_t = 1.0$, the third-order conditional structure functions of the thermodynamic variables are nearly constant in the range $16 \leqslant r/\eta \leqslant 64$, demonstrating the significant effect of the shocklet. We also show that, approximately, there is a very narrow power-law scaling with the scaling exponent close to 1.0 for the third-order structure functions of thermodynamic variables. Values of the scaling exponent other than 1.0 are also possible. It remains a challenge to obtain more exact scalings of the third-order structure functions in the inertial range.

Now we plot the conditional structure functions of the compressible velocity component and pressure $J_n^{L,c}$ and J_n^p, respectively, at $M_t = 1.0$ in Fig. 8, where $n \leqslant 6$. We show that $J_n^{L,c}$ is nearly constant in the range $4 \leqslant \eta \leqslant 32$ and J_n^p is nearly constant in the range $16 \leqslant \eta \leqslant 64$, as indicated by two dashed lines in the figure.

In order to obtain better scaling behaviors of the structure functions, we apply the extended self-similarity (ESS) analysis [26] to study the relative scaling behaviors of the structure functions of the compressible velocity component and thermodynamic variables. The ESS method is based on the following fact: Provided that structure functions exhibit some power-law scaling behaviors $S_n(r) \sim r^{\zeta_n}$, there are relative scaling behaviors between different orders of structure functions: $S_n(r) \sim [S_m(r)]^{\zeta_n/\zeta_m}$. Interestingly, there are wider scaling regions for the relative scaling behaviors,

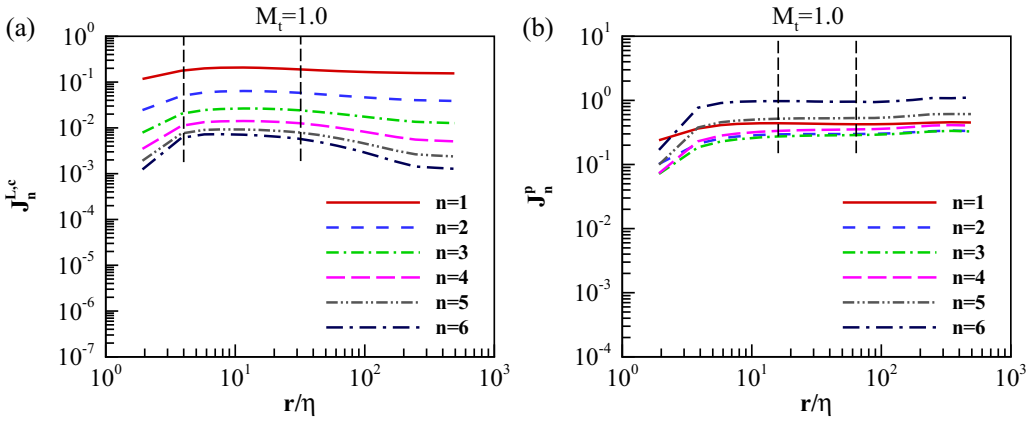

FIG. 8. Conditional structure functions of the compressible velocity and pressure at $M_t = 1.0$.

with the same scaling exponents ζ_n/ζ_m, as compared with the normal self-similarity scaling behaviors [26,27]. In compressible turbulence at high turbulent Mach numbers, there are two types of singular structures, intensive vortices and shocklets, which are similar to intensive vortices in incompressible turbulence and shock waves in Burgers turbulence, respectively. Since the ESS method works for both incompressible turbulence and Burgers turbulence [26,27], it is reasonable to expect that it also works for compressible turbulence.

We plot the structure functions of the compressible velocity component and thermodynamic variables against the third-order structure functions at $M_t = 1.0$ in Fig. 9. We mark out the range $4 \leqslant r/\eta \leqslant 32$ by two dashed lines for $S_n^{L,c}$, wherein the conditional structure function $J_n^{L,c}$ is nearly constant. We also mark out the range $16 \leqslant r/\eta \leqslant 64$ by two dashed lines for S_n^p, wherein the conditional structure function J_n^p is nearly constant. A general observation is that the shapes of all structure functions become nearly fixed at higher orders, indicating the saturation of scaling exponent at higher orders.

We calculate the extended self-similarity relative scaling exponents as shown in Fig. 10. The relative exponent of the compressible velocity component becomes nearly constant at high orders $n \geqslant 3$ with the saturated value $\zeta_\infty^{L,c}/\zeta_3^{L,c} \approx 1$. This observation demonstrates the similarity between

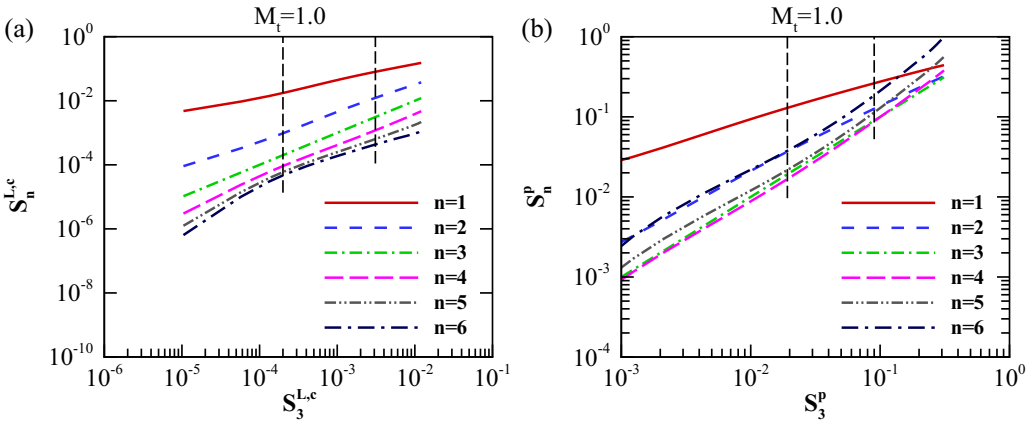

FIG. 9. Structure functions of the compressible velocity and pressure versus the third-order structure functions at $M_t = 1.0$.

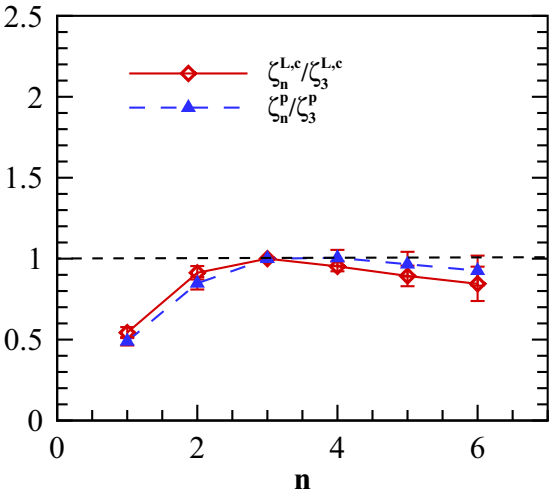

FIG. 10. Extended self-similarity relative scaling exponents of the compressible velocity and pressure at $M_t = 1.0$. Errors include both statistical fluctuations and the uncertainty in the fit to the power-law scaling range.

the compressible velocity component of the compressible turbulence and the velocity field in Burgers turbulence. We also observe the saturation of the relative scaling exponent of the pressure at high orders $n \geqslant 3$. The saturated relative scaling exponent is close to 1: $\zeta_\infty^p/\zeta_3^p \approx 1$. In a previous study, Benzi *et al.* pointed out that in the weakly compressible turbulence at an average Mach number close to 0.3, there are frontlike structures of the density although no shocks are produced, which gives rise to the saturation of the scaling exponents of the structure functions [33]. In particular, the structure functions of the density and pressure were found to have the saturation exponent 1.62 [33].

For the increment of the compressible velocity $\delta_r u^c(\mathbf{x}) = [\mathbf{u}^c(\mathbf{x}+\mathbf{r}) - \mathbf{u}^c(\mathbf{x})] \cdot \hat{\mathbf{r}}$, we consider the conditional PDF of the normalized increment of the compressible velocity $P_{\rm cond}(\delta_r u^c/u^{c,\rm rms})$ across a shocklet, namely, the PDF of $\delta_r u^c(\mathbf{x})/u^{c,\rm rms}$ where the flow fields satisfy the following conditions: $\nabla^2\rho(\mathbf{y}) = 0$, $\theta(\mathbf{y}) < -R_\theta\theta'$, and $\mathbf{y} = \mathbf{x} + \mathbf{r}/2$. Here R_θ is set to 3 unless noted otherwise. Similarly, we also consider the conditional PDFs of the normalized increments of the pressure, density, and temperature: $P_{\rm cond}(\delta_r p/p^{\rm rms})$, $P_{\rm cond}(\delta_r \rho/\rho^{\rm rms})$, and $P_{\rm cond}(\delta_r T/T^{\rm rms})$. Here $u^{c,\rm rms}$, $p^{\rm rms}$, $\rho^{\rm rms}$, and $T^{\rm rms}$ are rms values of the compressible velocity, pressure, density, and temperature, respectively. We plot conditional PDFs of the normalized increments of the compressible velocity, pressure, density, and temperature at $M_t = 1.0$ in Fig. 11. Since the left tails of $P_{\rm cond}(\delta_r u^c/u^{c,\rm rms})$ are longer than the right tails, the high-order moments of the normalized increments $\delta_r u^c/u^{c,\rm rms}$ are determined by the left tails. Moreover, the left tails of $P_{\rm cond}(\delta_r u^c/u^{c,\rm rms})$ overlap one another for different separations $4 \leqslant r/\eta \leqslant 64$. This observation is consistent with the previous result that the conditional structure function $J_n^{L,c}$ is nearly constant in the range $4 \leqslant \eta \leqslant 32$. Similarly, the tails of $P_{\rm cond}(\delta_r \rho/\rho^{\rm rms})$ and $P_{\rm cond}(\delta_r T/T^{\rm rms})$ overlap one another for different separations $8 \leqslant r/\eta \leqslant 96$, which is consistent with the previous observation that the conditional structure function J_n^p is nearly constant in the range $16 \leqslant \eta \leqslant 64$.

We employ exponential fitting functions for the left tails of conditional PDFs:

$$P_{\rm cond}(f) = C_1 \exp(-\beta|f|), \tag{35}$$

where f denotes the normalized increments of the compressible velocity, pressure, density, and temperature. The exponential fitting functions are plotted by solid lines in Fig. 11, showing good agreement with the results from the numerical simulations. The parameters C_1 and β are listed in Table II. The exponent β satisfies $1.0 < \beta < 2.0$.

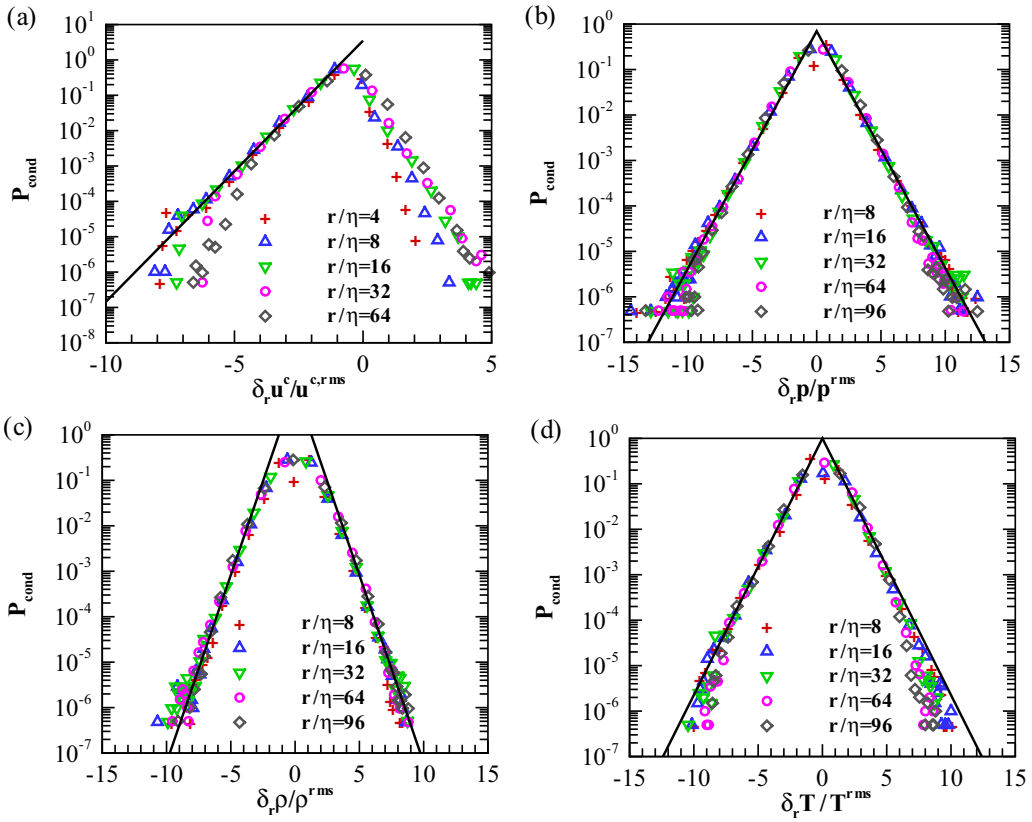

FIG. 11. Conditional PDFs of the normalized increments of the compressible velocity, pressure, density, and temperature at $M_t = 1.0$. Solid lines represent the exponential fitting function.

We now consider the PDFs of the normalized increments of the compressible velocity, pressure, density, and temperature: $P(\delta_r u^c/u^{c,\mathrm{rms}})$, $P(\delta_r p/p^{\mathrm{rms}})$, $P(\delta_r \rho/\rho^{\mathrm{rms}})$, and $P(\delta_r T/T^{\mathrm{rms}})$. In Fig. 12 we present the normalized PDFs of the increments of the compressible velocity, pressure, density, and temperature: $(r/\eta)^{-1}P(\delta_r u^c/u^{c,\mathrm{rms}})$, $(r/\eta)^{-1}P(\delta_r p/p^{\mathrm{rms}})$, $(r/\eta)^{-1}P(\delta_r \rho/\rho^{\mathrm{rms}})$, and $(r/\eta)^{-1}P(\delta_r T/T^{\mathrm{rms}})$. The tails of the normalized PDFs of the increments of the pressure, density and temperature nearly overlap one another for different separations r/η in the range of $8 \leqslant r/\eta \leqslant 96$.

The situation of the compressible velocity is interesting: The left tails of the normalized PDFs $(r/\eta)^{-1}P(\delta_r u^c/u^{c,\mathrm{rms}})$ overlap one another for different separations $4 \leqslant r/\eta \leqslant 64$, while the right tails are quite scattered. The left tail of the normalized PDF $(r/\eta)^{-1}P(\delta_r u^c/u^{c,\mathrm{rms}})$ is much longer

TABLE II. Parameters of the fitting functions for the exponential tails of conditional PDFs and unconditional PDFs.

Variable	β	C_1	C_2	$C_0 = C_1/C_2$
$\delta_r u^c/u^{c,\mathrm{rms}}$	1.7	3.5	0.009	3.9×10^2
$\delta_r p/p^{\mathrm{rms}}$	1.2	0.7	0.0018	3.9×10^2
$\delta_r \rho/\rho^{\mathrm{rms}}$	1.9	11	0.028	3.9×10^2
$\delta_r T/T^{\mathrm{rms}}$	1.3	1.0	0.0026	3.8×10^2

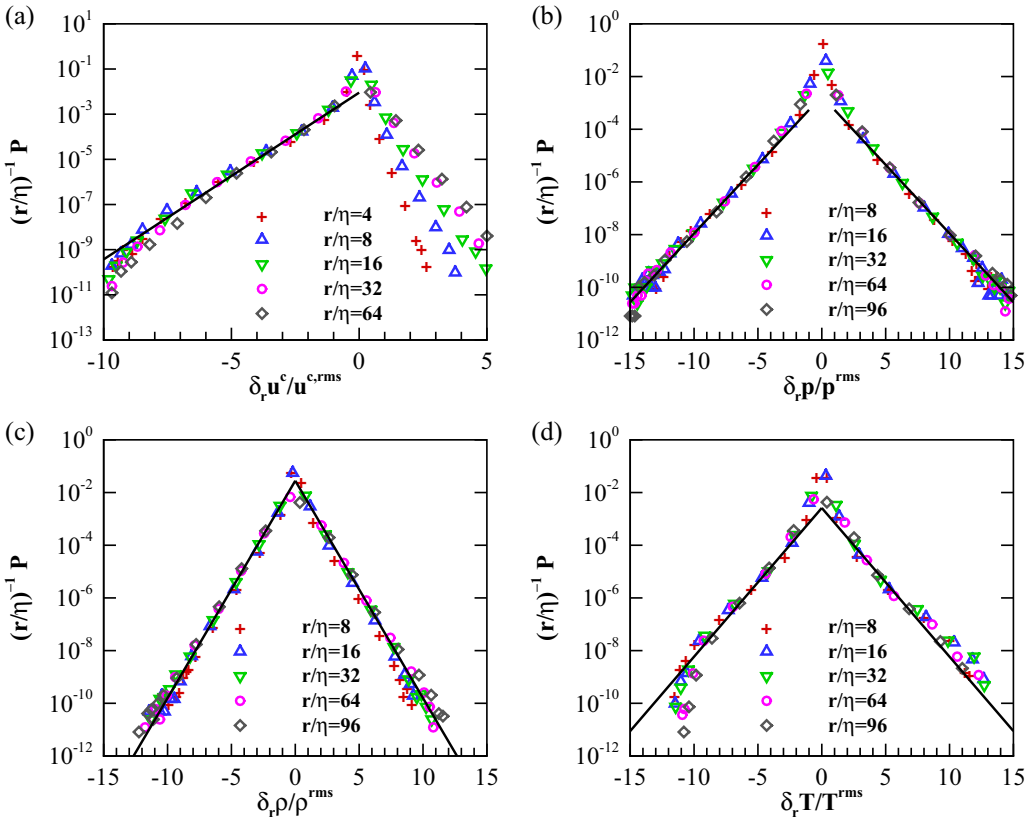

FIG. 12. Normalized PDFs of the increments of the compressible velocity, pressure, density and temperature at $M_t = 1.0$. Solid lines represent the exponential fitting function.

than the right tail, particularly at small separations. Thus, the left tail has a major contribution to the high-order structure functions of the compressible velocity $S_n^{L,c}(r)$.

We employ exponential fitting functions for the left tails of PDFs:

$$(r/\eta)^{-1} P(f) = C_2 \exp(-\beta |f|), \tag{36}$$

where f denotes the normalized increments of the compressible velocity, pressure, density, and temperature. We show that the exponent β of the normalized PDF $(r/\eta)^{-1} P$ is the same as that for the conditional PDF $P_{\rm cond}$. The exponential fitting functions are plotted by solid lines in Fig. 12, showing good agreement with the results from the numerical simulations. The parameters C_2 and β are listed in Table II. We calculate the ratio $C_0 = C_1/C_2$: $C_0 \approx 3.9 \times 10^2$ for the normalized increments of the compressible velocity, pressure, and density and $C_0 \approx 3.8 \times 10^2$ for the normalized increment of the temperature.

We propose the following scenario based on the multifractal theory [10,33–35]. Sheetlike shocklets in the simulated flow play a significant role in the fluctuations of the compressible velocity and thermodynamic variables. Specifically, provided that the fluctuations of g (which denotes the compressible velocity, pressure, density, and temperature) are large enough, they would be simply characterized by $g(x+r) - g(x) \sim C_g$ for $x+r$ and x on two different sides of a shocklet and $g(x+r) - g(x) \sim 0$ if there is no shocklet between the two points $x+r$ and x. The constant C_g is dependent on the strength of the shocklet but is nearly independent on the separation r. A PDF of C_g is merely the conditional PDF $P_{\rm cond}$. The probability of a shocklet being located between two arbitrarily selected points $x+r$ and x is proportional to the separation r, giving rise to

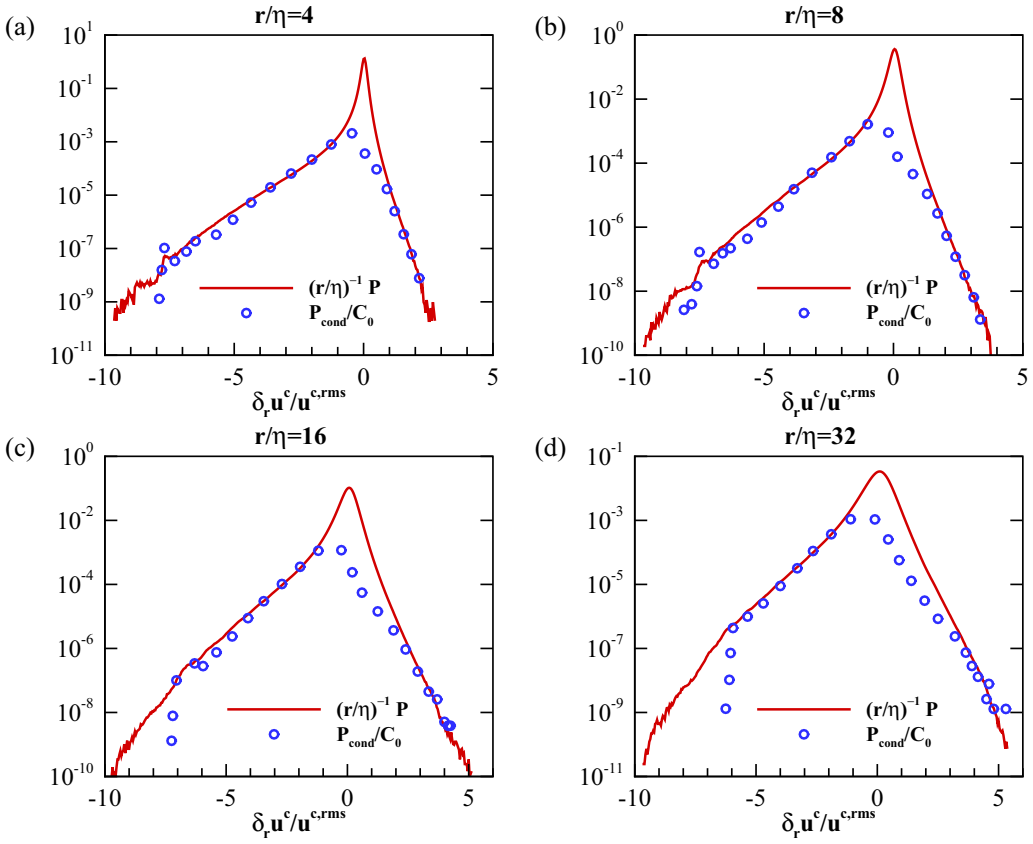

FIG. 13. Conditional PDFs and normalized PDFs of the increment of the compressible velocity at $M_t = 1.0$: (a) $r/\eta = 4$, (b) $r/\eta = 8$, (c) $r/\eta = 16$, and (d) $r/\eta = 32$.

$g(x+r) - g(x) \sim C_g r/L_s$ in the simulated flow. Here L_s is the characteristic length scale for the locations of the shocklets. Thus, the PDF of $g(x+r) - g(x)$ can be related to the conditional PDF as $P = P_{\text{cond}} r/L_s$. Therefore, we obtain

$$(r/\eta)^{-1} P = P_{\text{cond}}/C_0, \tag{37}$$

where $C_0 = L_s/\eta$. From the previous calculations, we show that $L_s/\eta \approx 3.9 \times 10^2$. It is worth noting that L_s is in proportional to the average distance between two neighboring shocklets. Provided that $r \leqslant L_s$, the probability for a shocklet locating between two arbitrarily selected points $x + r$ and x is approximately equal to r/L_s. Equation (37) is no longer reliable for $r \geqslant L_s$. From numerical results as shown in Fig. 12 and Table II, Eq. (37) is verified at $8 \leqslant r/\eta \leqslant 64$.

We plot conditional PDFs and normalized PDFs of the increments of the compressible velocity at $M_t = 1.0$ in Fig. 13. The left tail of $(r/\eta)^{-1} P$ can be well approximated by P_{cond}/C_0. As the separation r increases, the right tail of $(r/\eta)^{-1} P$ becomes wider and the difference between two right tails of $(r/\eta)^{-1} P$ and P_{cond}/C_0 become larger. This observation implies that the effect of flow structures other than the shocklet on the right tail of $(r/\eta)^{-1} P$ is significant.

To sum up, collapse of the tails of the PDFs of the increments of the compressible velocity and pressure by proper normalization indicates the saturation of the scaling exponents $\zeta_n^{L,c}$ and ζ_n^p at high orders, based on the multifractal theory [33,34]. The observations are consistent with the previous visualizations of the sheetlike isosurfaces of the velocity divergence and the pressure gradient in Fig. 2. Sheetlike structures indicate that the geometrical dimension of the spatial distribution of large

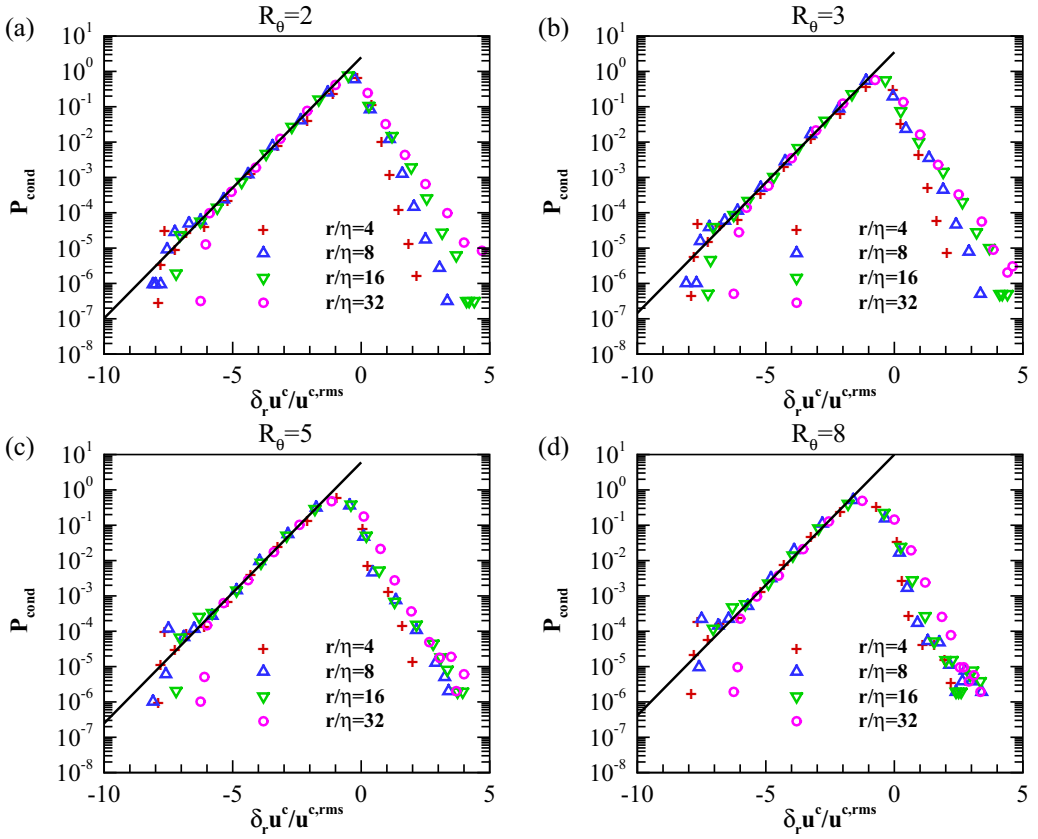

FIG. 14. Conditional PDFs of the normalized increments of the compressible velocity at $M_t = 1.0$ for different threshold R_θ: (a) $R_\theta = 2$, (b) $R_\theta = 3$, (c) $R_\theta = 5$, and (d) $R_\theta = 8$. Solid lines represent the exponential fitting function.

jumps (singular structures) equals 2 for the compressible velocity component, density, pressure, and temperature. Therefore, the scaling exponents of high-order structure functions have a saturation value of 1.

Now we investigate the effect of the threshold R_θ on the conditional PDFs of the normalized increments of the compressible velocity. We plot $P_{\rm cond}(\delta_r u^c/u^{c,{\rm rms}})$ at $M_t = 1.0$ for different values of the threshold R_θ in Fig. 14. We observe that the left tails of $P_{\rm cond}(\delta_r u^c/u^{c,{\rm rms}})$ overlap one another at different separations $4 \leqslant r/\eta \leqslant 32$ for $R_\theta = 2$, 3, 5, and 8. We apply the exponential fitting functions (35) for the left tails of $P_{\rm cond}(\delta_r u^c/u^{c,{\rm rms}})$. The exponential fitting functions are plotted by solid lines in Fig. 14, which are consistent with the numerical results. The parameters β, C_1, and C_0 are listed in Table III. It is shown that the exponent β does not depend on the threshold

TABLE III. Parameters of the fitting functions for conditional PDFs at different threshold R_θ.

Variable	R_θ	β	C_1	$C_0 = C_1/C_2$
$\delta_r u^c/u^{c,{\rm rms}}$	2	1.7	2.5	2.8×10^2
$\delta_r u^c/u^{c,{\rm rms}}$	3	1.7	3.5	3.9×10^2
$\delta_r u^c/u^{c,{\rm rms}}$	5	1.7	6.0	6.7×10^2
$\delta_r u^c/u^{c,{\rm rms}}$	8	1.7	10.0	1.1×10^3

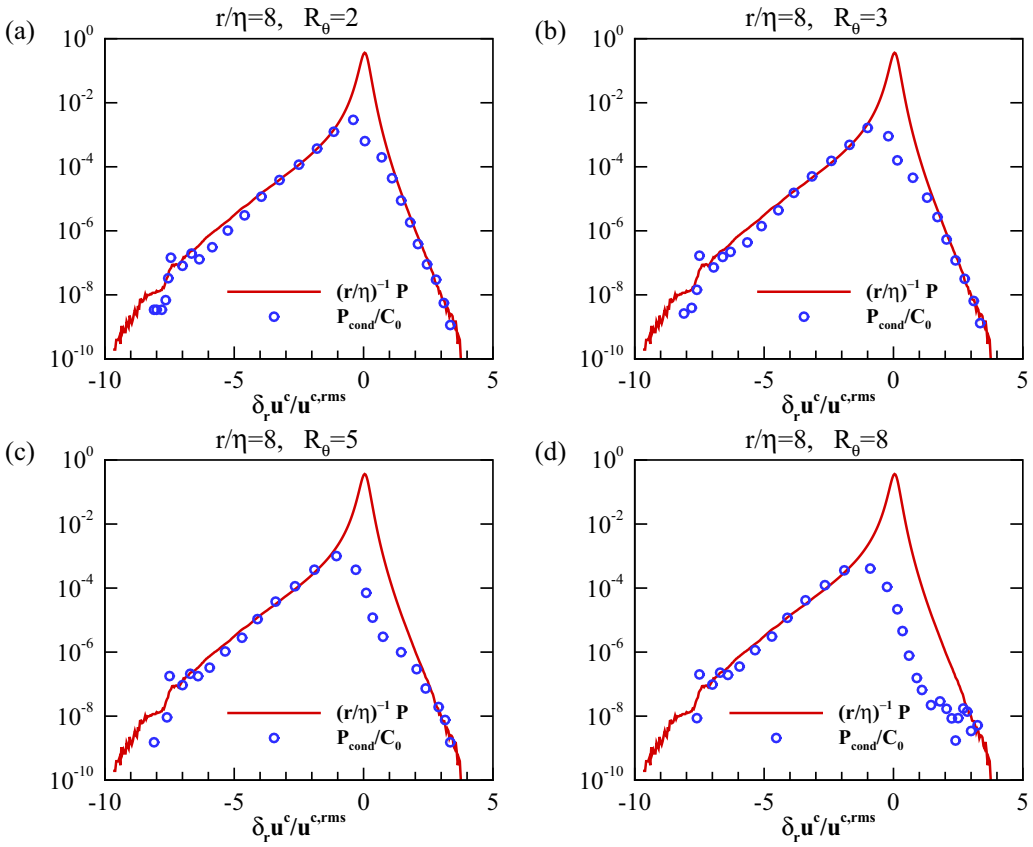

FIG. 15. Conditional PDFs and normalized PDFs of the increment of the compressible velocity at $M_t = 1.0$ for different threshold R_θ: (a) $R_\theta = 2$, (b) $R_\theta = 3$, (c) $R_\theta = 5$, and (d) $R_\theta = 8$.

R_θ. The parameters C_1 and C_0 become larger with the increase of R_θ. The ratio C_1/R_θ satisfies $1.16 \leqslant C_1/R_\theta \leqslant 1.25$. According to Eq. (37), the parameter C_0 represents the ratio of the length scale L_s to the Kolmogorov scale η: $C_0 = L_s/\eta$, where L_s is in proportional to the average distance between two neighboring shocklet. As the threshold R_θ increases, the number of shocklets becomes smaller and the length scale L_s becomes larger, leading to the increase of parameter C_0.

We plot conditional PDFs and normalized PDFs of the increment of the compressible velocity at $r/\eta = 8$ and $M_t = 1.0$ for different values of the threshold R_θ in Fig. 15. It is shown that the left tail of $(r/\eta)^{-1}P$ can be well approximated by $P_{\rm cond}/C_0$ for $R_\theta = 2$, 3, 5, and 8. As the threshold R_θ increases, the difference between two right tails of $(r/\eta)^{-1}P$ and $P_{\rm cond}/C_0$ becomes larger. This observation implies that the statistics of very strong shocklets with $R_\theta \geqslant 5$ is not enough to capture the right tail of $(r/\eta)^{-1}P$.

It is worth noting that the left tail of the PDF of the velocity divergence characterizes compression motion, while the right tail of the PDF of the velocity divergence characterizes expansion motion. We argue that the effect of shock waves is mainly concentrated on the left tails of $P(\delta_r u^c/u^{c,\rm rms})$, while the effect of expansionlike waves is mainly concentrated on the right tails of $P(\delta_r u^c/u^{c,\rm rms})$. Since the effect of shock waves dominates over expansion waves, the scaling behavior of the overall compressible velocity is similar to Burgers turbulence.

Moreover, we decompose the compressible velocity increment $\delta_r u^c$ into a negative component $\delta_r u^{c,N}$ and a positive component $\delta_r u^{c,P}$: $\delta_r u^c = \delta_r u^{c,N} + \delta_r u^{c,P}$. Here $\delta_r u^{c,N} = \delta_r u^c$ if $\delta_r u^c \leqslant 0$; otherwise $\delta_r u^{c,N} = 0$. Similarly, $\delta_r u^{c,P} = \delta_r u^c$ if $\delta_r u^c \geqslant 0$; otherwise $\delta_r u^{c,P} = 0$. Similar

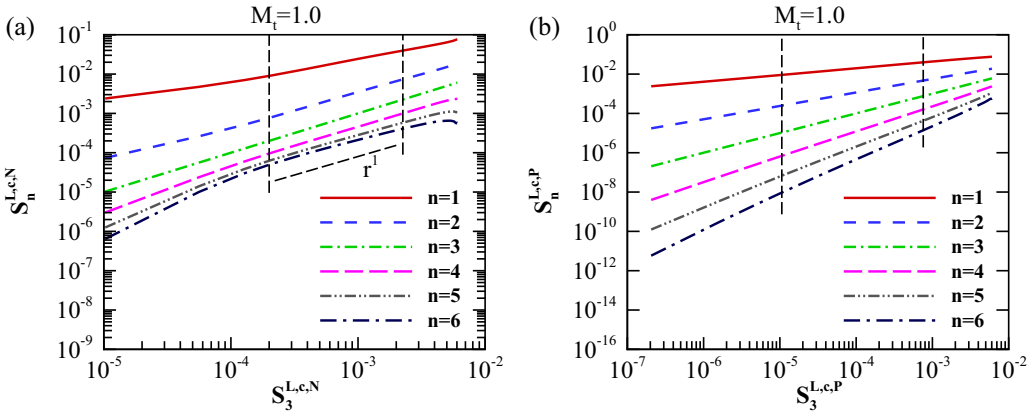

FIG. 16. Structure functions of the negative component and positive component of the increment of the compressible velocity at $M_t = 1.0$.

decompositions already have been used in some studies of one-dimensional Burgers turbulence [36,37] and one-dimensional compressible turbulence [38]. We define the structure functions for the two components of the compressible velocity increment as

$$S_n^{L,c,N}(r) \equiv \left\langle \left| \frac{1}{u'} \delta_r u^{c,N} \right|^n \right\rangle, \tag{38}$$

$$S_n^{L,c,P}(r) \equiv \left\langle \left| \frac{1}{u'} \delta_r u^{c,P} \right|^n \right\rangle. \tag{39}$$

We plot the structure functions $S_n^{L,c,N}$ and $S_n^{L,c,P}$ as functions of $S_3^{L,c,N}$ and $S_3^{L,c,P}$, respectively, in Fig. 16. The range of $4 \leqslant r/\eta \leqslant 32$ is indicated by two dash-dotted lines. We observe good relative scaling behaviors for both $S_n^{L,c,N}$ and $S_n^{L,c,P}$. The difference between $S_n^{L,c,N}$ and $S_n^{L,c,P}$ is quite large, due to the different mechanisms of shock waves and expansionlike waves. We report the relative scaling exponents in Fig. 17. We find that the relative scaling exponent $\zeta_n^{L,c,N}/\zeta_3^{L,c,N}$

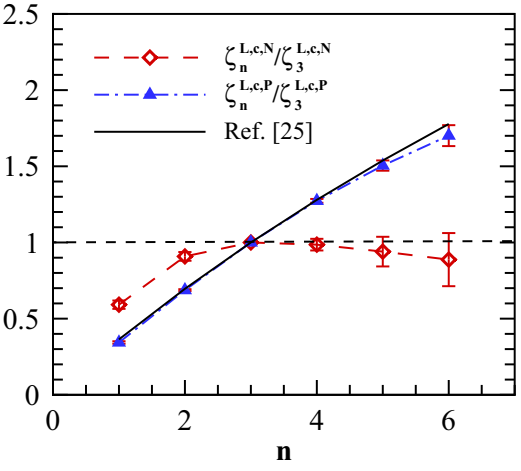

FIG. 17. Relative scaling exponents for the negative component and positive component of the increment of the compressible velocity at $M_t = 1.0$.

exhibits a scaling behavior with the saturation of the scaling exponent at high orders, which is similar to that of the velocity field in Burgers turbulence, while the relative scaling exponent $\zeta_n^{L,c,P}/\zeta_3^{L,c,P}$ is close to the She-Leveque model of incompressible turbulence [25]. The statistics of the negative component $\delta_r u^{c,N}$ of the compressible velocity increment is associated with the left tail of the PDF $P(\delta_r u^c/u^{c,\mathrm{rms}})$. We have shown that the left tail of the PDF $P(\delta_r u^c/u^{c,\mathrm{rms}})$ is well approximated by Eq. (37), which is based on the assumption that shocklets play a significant role in the fluctuations of the compressible velocity. Thus, the structure functions $S_n^{L,c,N}$ exhibit the scaling relation $S_n^{L,c,N}(r) \sim r$ at high orders. The statistics of the positive component $\delta_r u^{c,P}$ of the compressible velocity increment is associated with the right tail of the PDF $P(\delta_r u^c/u^{c,\mathrm{rms}})$. We have shown that the effect of flow structures other than the shocklet on the right tail of the PDF $P(\delta_r u^c/u^{c,\mathrm{rms}})$ is significant. The most dissipative structures associated with expansion waves are different from the sheetlike dissipative structures associated with shocklets [19,25]. Thus, the scaling exponents of the high-order moments of $\delta_r u^{c,P}$ are different from those of $\delta_r u^{c,N}$. Interestingly, in a previous work by Zhang and She [37], it was shown that the rarefaction wave subensemble does not exhibit any intermittency and satisfies the Kolmogorov scaling law in one-dimensional Burgers turbulence. Here we infer that the effect of local rapid rarefaction wave on the relative scaling exponents $\zeta_n^{L,c,P}/\zeta_3^{L,c,P}$ in three-dimensional compressible turbulence is similar to the effect of vortex filament on the scaling exponents of velocity structure functions in three-dimensional incompressible turbulence [25].

V. CONCLUSION

In this paper we investigated scaling and intermittency in solenoidally forced compressible isotropic turbulence at the turbulent Mach number M_t from 0.5 to 1.0 and at the Taylor Reynolds number $\mathrm{Re}_\lambda \approx 250$. We showed that the relations between the structure functions of the solenoidal velocity and pressure are similar to incompressible turbulence and found that there exist linear relations among the second-order structure functions of the compressible velocity, density, pressure, and temperature by numerical simulations. We developed models of the structure function relations, based on the ideal shock jump conditions, which were found to be consistent with the numerical results of the structure functions at the second order.

We studied the conditional structure functions of the velocity and thermodynamic variables with respect to the shocklet. Both the conditional and unconditional structure functions of the compressible velocity and thermodynamic variables are nearly identical at large scales $r/\eta \geqslant 300$. The difference between the conditional and unconditional structure functions increases rapidly as the separation r becomes smaller and as the turbulent Mach number becomes larger. We reported that plateau regions of the conditional structure functions gradually develop as the turbulent Mach number increases. In particular, at $M_t = 1.0$, we observed that the conditional structure functions have only a slight dependence on the separation r in the range of $r/\eta \geqslant 4$.

We applied the extended self-similarity analysis to study the scaling behavior of the structure functions of the compressible velocity and pressure at $M_t = 1.0$. The relative scaling exponents of the structure functions obtained by the ESS were found to be saturated at high orders, similar to Burgers turbulence. We observed that after proper normalization, the left tails of the PDFs of the increments of the compressible velocity component and the tails of PDFs of the increments of pressure overlap one another for different separations r. We also studied the conditional PDFs of the increments with respect to the shocklet. The tails of the conditional PDFs were found to overlap one another for different separations. Based on a simple scenario for the fluctuations of variables across the shocklet, linear relations between the tails of the normalized PDFs and conditional PDFs were established, which were confirmed by numerical simulations. It was shown that the shocklet plays an important role in the determination of the PDF tails.

The compressible velocity increment was decomposed into a negative component and a positive component. The negative component of the compressible velocity increment exhibits a scaling

behavior with the saturation of scaling exponent at high orders, which is similar to Burgers turbulence. The positive component exhibits a scaling behavior that is similar to incompressible turbulence.

Finally, we emphasize that numerical simulations at higher grid resolutions and higher Reynolds numbers are required to further study the scaling behaviors of structure functions of the compressible velocity and thermodynamic variables, which are certainly a challenge to turbulence study.

ACKNOWLEDGMENTS

The authors gratefully acknowledge valuable discussions with Dr. Jingyuan Yang, Dr. Yantao Yang, and Professor Shiyi Chen. The authors also appreciate valuable comments by the anonymous referees. The numerical simulations were done on the supercomputer at Nagoya University. The works of T.G. and T.W. were supported by JSPS KAKENHI Grants No. 15H02218 and No. 26420106, respectively. J.W. acknowledges Dr. Izumi Saito for considerable help using the supercomputer at Nagoya University.

[1] P. Sagaut and C. Cambon, *Homogeneous Turbulence Dynamics* (Cambridge University Press, Cambridge, 2008).
[2] R. Samtaney, D. I. Pullin, and B. Kosovic, Direct numerical simulation of decaying compressible turbulence and shocklet statistics, Phys. Fluids **13**, 1415 (2001).
[3] S. Pirozzoli and F. Grasso, Direct numerical simulations of isotropic compressible turbulence: Influence of compressibility on dynamics and structures, Phys. Fluids **16**, 4386 (2004).
[4] M. R. Petersen and D. Livescu, Forcing for statistically stationary compressible isotropic turbulence, Phys. Fluids **22**, 116101 (2010).
[5] J. Wang, Y. Shi, L.-P. Wang, Z. Xiao, X. T. He, and S. Chen, Effect of shocklets on the velocity gradients in highly compressible isotropic turbulence, Phys. Fluids **23**, 125103 (2011).
[6] J. Wang, Y. Shi, L.-P. Wang, Z. Xiao, X. T. He, and S. Chen, Effect of compressibility on the small scale structures in isotropic turbulence, J. Fluid Mech. **713**, 588 (2012).
[7] J. Wang, Y. Shi, L.-P. Wang, Z. Xiao, X. T. He, and S. Chen, Scaling and Statistics in Three-Dimensional Compressible Turbulence, Phys. Rev. Lett. **108**, 214505 (2012).
[8] D. A. Donzis and S. Jagannathan, Fluctuations of thermodynamic variables in stationary compressible turbulence, J. Fluid Mech. **733**, 221 (2013).
[9] S. Jagannathan and D. A. Donzis, Reynolds and Mach number scaling in solenoidally-forced compressible turbulence using high-resolution direct numerical simulations, J. Fluid Mech. **789**, 669 (2016).
[10] Y. Yang, J. Wang, Y. Shi, Z. Xiao, X. T. He, and S. Chen, Intermittency caused by compressibility: A Lagrangian study, J. Fluid Mech. **786**, R6 (2016).
[11] Z. Xia, Y. Shi, Q. Zhang, and S. Chen, Modulation to compressible homogenous turbulence by heavy point particles. I. Effect of particles' density, Phys. Fluids **28**, 016103 (2016).
[12] Q. Zhang, H. Liu, Z. Ma, and Z. Xiao, Preferential concentration of heavy particles in compressible isotropic turbulence, Phys. Fluids **28**, 055104 (2016).
[13] J. Wang, T. Gotoh, and T. Watanabe, Spectra and statistics in compressible isotropic turbulence, Phys. Rev. Fluids **2**, 013403 (2017).
[14] J. Wang, T. Gotoh, and T. Watanabe, Shocklet statistics in compressible isotropic turbulence, Phys. Rev. Fluids **2**, 023401 (2017).
[15] H. Aluie, Compressible Turbulence: The Cascade and its Locality, Phys. Rev. Lett. **106**, 174502 (2011).
[16] S. Galtier and S. Banerjee, Exact Relation for Correlation Functions in Compressible Isothermal Turbulence, Phys. Rev. Lett. **107**, 134501 (2011).
[17] J. Wang, Y. Yang, Y. Shi, Z. Xiao, X. He, and S. Chen, Cascade of Kinetic Energy in Three-Dimensional Compressible Turbulence, Phys. Rev. Lett. **110**, 214505 (2013).

[18] A. G. Kritsuk, R. Wagner, and M. L. Norman, Energy cascade and scaling in supersonic isothermal turbulence, J. Fluid Mech. **729**, R1 (2013).
[19] S. Boldyrev, A. Nordlund, and P. Padoan, Scaling relations of supersonic turbulence in star-forming molecular clouds, Astrophys. J. **573**, 678 (2002).
[20] S. Boldyrev, A. Nordlund, and P. Padoan, Supersonic Turbulence and Structure of Interstellar Molecular Clouds, Phys. Rev. Lett. **89**, 031102 (2002).
[21] A. Kritsuk, M. Norman, P. Padoan, and R. Wagner, The statistics of supersonic isothermal turbulence, Astrophys. J. **665**, 416 (2007).
[22] W. Schmidt, C. Federrath, and R. Klessen, Is the Scaling of Supersonic Turbulence Universal? Phys. Rev. Lett. **101**, 194505 (2008).
[23] L. Konstandin, C. Federrath, R. Klessen, and W. Schmidt, Statistical properties of supersonic turbulence in the Lagrangian and Eulerian frameworks, J. Fluid Mech. **692**, 183 (2012).
[24] C. Federrath, On the universality of supersonic turbulence, Mon. Not. R. Astron. Soc. **436**, 1245 (2013).
[25] Z. She and E. Leveque, Universal Scaling Laws in Fully Developed Turbulence, Phys. Rev. Lett. **72**, 336 (1994).
[26] R. Benzi, S. Ciliberto, R. Tripiccione, C. Baudet, F. Massaioli, and S. Succi, Extended self-similarity in turbulent flows, Phys. Rev. E **48**, R29 (1993).
[27] S. Chakraborty, U. Frisch, and S. S. Ray, Extended self-similarity works for the Burgers equation and why, J. Fluid Mech. **649**, 275 (2010).
[28] J. Wang, L.-P. Wang, Z. Xiao, Y. Shi, and S. Chen, A hybrid numerical simulation of isotropic compressible turbulence, J. Comput. Phys. **229**, 5257 (2010).
[29] S. K. Lele, Compact finite difference schemes with spectral-like resolution, J. Comput. Phys. **103**, 16 (1992).
[30] D. S. Balsara and C. W. Shu, Monotonicity preserving weighted essentially non-oscillatory schemes with increasingly high order of accuracy, J. Comput. Phys. **160**, 405 (2000).
[31] T. Ishihara, Y. Kaneda, M. Yokokawa, K. Itakura, and A. Uno, Small-scale statistics in high-resolution direct numerical simulation of turbulence: Reynolds number dependence of one-point velocity gradient statistics, J. Fluid Mech. **592**, 335 (2007).
[32] N. Cao, S. Chen, and G. D. Doolen, Statistics and structures of pressure in isotropic turbulence, Phys. Fluids **11**, 2235 (1999).
[33] R. Benzi, L. Biferale, R. T. Fisher, L. P. Kadanoff, D. Q. Lamb, and F. Toschi, Intermittency and Universality in Fully Developed Inviscid and Weakly Compressible Turbulent Flows, Phys. Rev. Lett. **100**, 234503 (2008).
[34] T. Watanabe and T. Gotoh, Intermittency in passive scalar turbulence under the uniform mean scalar gradient, Phys. Fluids **18**, 058105 (2006).
[35] J. Wang, Y. Yang, Y. Shi, Z. Xiao, X. He, and S. Chen, Statistics and structures of pressure and density in compressible isotropic turbulence, J. Turbul. **14**, 21 (2013).
[36] D. Mitra, J. Bec, R. Pandit, and U. Frisch, Is Multiscaling an Artifact in the Stochastically Forced Burgers Equation? Phys. Rev. Lett. **94**, 194501 (2005).
[37] Z. Zhang and Z. She, Subensemble decomposition and Markov process analysis of Burgers turbulence, Phys. Rev. E **84**, 026326 (2011).
[38] Q. Ni, Y. Shi, and S. Chen, Statistics of one-dimensional compressible turbulence with random large-scale force, Phys. Fluids **25**, 075106 (2013).